Journal of
Synchrotron Radiation

ISSN 0909-0495

Received 29 July 2011
Accepted 24 January 2012

Synchrotron-radiation phase-contrast imaging of human stomach and gastric cancer: *in vitro* studies

Lei Tang,[a] Gang Li,[b] Ying-Shi Sun,[a] Jie Li[a] and Xiao-Peng Zhang[a]*

[a]Key Laboratory of Carcinogenesis and Translational Research (Ministry of Education), Peking University School of Oncology, Beijing Cancer Hospital and Institute, No. 52 Fu Cheng Road, Hai Dian District, Beijing 100142, People's Republic of China, and [b]Beijing Synchrotron Radiation Facility, Institute of High Energy Physics, Chinese Academy of Sciences, Beijing 100049, People's Republic of China. E-mail: zxp@bjcancer.org

The electron density resolution of synchrotron-radiation phase-contrast imaging (SR-PCI) is 1000 times higher than that of conventional X-ray absorption imaging in light elements, through which high-resolution X-ray imaging of biological soft tissue can be achieved. For biological soft tissue, SR-PCI can give better imaging contrast than conventional X-ray absorption imaging. In this study, human resected stomach and gastric cancer were investigated using in-line holography and diffraction enhanced imaging at beamline 4W1A of the Beijing Synchrotron Radiation Facility. It was possible to depict gastric pits, measuring 50–70 μm, gastric grooves and tiny blood vessels in the submucosa layer by SR-PCI. The fine structure of a cancerous ulcer was displayed clearly on imaging the mucosa. The delamination of the gastric wall and infiltration of cancer in the submucosa layer were also demonstrated on cross-sectional imaging. In conclusion, SR-PCI can demonstrate the subtle structures of stomach and gastric cancer that cannot be detected by conventional X-ray absorption imaging, which prompt the X-ray diagnosis of gastric disease to the level of the gastric pit, and has the potential to provide new methods for the imageology of gastric cancer.

Keywords: phase contrast; X-ray; stomach; neoplasm.

1. Introduction

Gastric cancer is a type of malignant tumor with high prevalence and mortality rate worldwide (Parkin *et al.*, 2005). Early detection and diagnosis remains one of the key approaches to improving the prognosis of patients with gastric cancer (Han *et al.*, 2003). X-ray examination is one of the basic imaging modalities in the evaluation of gastric cancer. Conventional X-ray imaging in clinical practices mainly employs the absorption characteristics of X-rays, and discriminates different tissues through the linear attenuation coefficient (μ). The μ values of tissues are proportional to their density. In the case of a spatial resolution of 1–2 mm of conventional imaging modality, the lowest density difference that can be detected is only 0.01 g cm^{-3}. Therefore, although high contrast can evidently be achieved among tissues with different proportions of light and heavy elements (*e.g* bone *versus* muscle), it is difficult to discriminate the detailed structure difference in soft tissues which only contain light elements (*e.g* the gastric wall). The low-density contrast of X-ray absorption imaging became the main obstacle to the development of clinical practices (Takeda *et al.*, 2000; Reto *et al.*, 2004; Keyriläinen *et al.*, 2005; Kitchen *et al.*, 2005).

In order to compensate for the deficiency mentioned above, an oral double-contrast agent (gas and barium sulfate) is usually taken to increase the contrast during the clinical X-ray examination of gastric cancer. Owing to the high contrast between barium sulfate coated on the surface of the gastric mucosa and gas in the gastric lumen, the shape of the gastric mucosa is depicted indirectly by X-ray imaging. Limited by the deficiency of conventional absorption imaging, the minimal unit depicted by refined gastric double-contrast X-ray imaging is the gastric area with a mean size of 1–3 mm (Virkkunen & Retulainen, 1980). The detection and diagnosis of early gastric cancer, which is small in size, is therefore limited by the low resolution of conventional X-ray double-contrast imaging (Muto *et al.*, 2001).

Synchrotron-radiation hard X-ray phase-contrast imaging (SR-PCI) is a newly developed imaging modality. It employs phase-contrast information, which forms through the redistribution of light intensity when penetrating through tissues, and depends on the refractive index of different tissues to form contrast. According to the refractive index formula, $n = 1 - \delta - i\beta$, where $\delta = r_e\rho_e\lambda^2/2\pi$ and $\beta = \mu\lambda/4\pi$; δ is correlated with the phase and β is correlated with the absorption coefficient μ. Taking C_2H_4, for example, the phase-correlated

index δ of 25 keV X-rays (λ = 0.496 Å) is 3.5×10^{-7}, yet the absorption-correlated index β is 8.1×10^{-11}. δ is higher than β by about three to four magnitudes, and the phase contrast can reach 0.0003 g cm^{-3}. So the contrast of light elements can, in theory, reach 1000 times that of conventional absorption imaging (Takeda *et al.*, 2000; Reto *et al.*, 2004; Keyriläinen *et al.*, 2005; Kitchen *et al.*, 2005).

Based on the advantages mentioned above, SR-PCI promises broad prospects in domains such as biomedicine and material science. *In vitro* high-resolution SR-PCI had been performed on breast, lung, liver, kidney, *etc.* through which excellent soft tissue contrast can be achieved without enhancement agents (Takeda *et al.*, 1998, 2000; Reto *et al.*, 2004; Keyriläinen *et al.*, 2005; Kitchen *et al.*, 2005; Yagi *et al.*, 1999; Liu *et al.*, 2008). Yet there are still no reports of *in vitro* SR-PCI of stomach and gastric cancer. We have employed beamline 4W1A of the Beijing Synchrotron Radiation Facility (BSRF), Institute of High Energy Physics, Chinese Academy of Sciences, to study SR-PCI in stomach and gastric cancer *in vitro*, and have explored the ability of this new type of imaging modality to demonstrate fine structure in gastric wall layers and mucosa morphology.

2. Material and methods

2.1. Specimen preparation and imaging

One case of gastric antrum carcinoma was resected through an operation at Beijing Cancer Hospital. Four specimens, including three pieces of normal gastric wall and one piece of gastric cancer, were taken from the whole sample. The mucosa side was washed repeatedly to remove the coated mucus, and then soaked in 10% formalin solution for seven days. The specimens were fixed and the mucosa layer was stripped from the muscular propria layer using a scalpel along the submucosa. The intact mucosa layers were stretched and expanded, and intact 2 cm $\times$ 2 cm pieces were cut out from the central area and fixed onto a plastic foam plate using tacks. A cancerous ulcer specimen was stripped, starting from the nearby normal gastric submucosa, horizontally across the annular dike and reaching the bottom of the ulcer, keeping the cancerous part of thickness 2–5 mm, and fixed onto a plastic foam plate as above. Three pieces of cross-sectional tissues at the border of the gastric cancer and the normal gastric wall were cut into strips of thickness <5 mm. Then the prepared specimens were soaked in 10% formalin solution for another three days. The specimens were placed on a fixing frame, and a reverse projection method using visible light was employed to determine the imaging area.

2.2. SR-PCI

SR-PCI of tumor specimens was performed at beamline 4W1A of the BSRF. The synchrotron radiation source of 4W1A is a single-period wavelength shifter characterized by a magnetic period length of 1.39 m, a peak magnetic field of 1.8 T and a gap of 66 mm. When the storage ring is working with an electron energy of 2.2 GeV, its critical energy is 5.8 keV. During synchrotron-radiation-dedicated shifts, the electron bunch size is s_x = 0.78 mm and s_y = 0.28 mm. The total acceptance angle is 1.0 mrad in the horizontal direction and 0.3 mrad in the vertical direction.

Both diffraction enhanced imaging (DEI) and in-line holography were used in this experiment. The DEI method uses one or a pair of crystals (analytical crystals) placed between the sample and the detector to remove the scattered light from refracted and transmitted light. When monochromatic X-rays cross the samples, they will generate a chart depicting the distribution of different angular refraction, which is related to the gradient of the phase. Because the boundary of optical constants will produce an enhanced contrast, a very clear and rich detailed image can be generated on a weak absorber, which greatly enhances the density contrast resolution. The DEI method normally requires monochromatic incident X rays with small divergence, and very precise analytic crystal orientation control equipment.

In order to obtain a high degree of monochromatic and parallel incident light, multi-block crystals have been used in other reports (Dilmanian *et al.*, 2000; Oltulu *et al.*, 2003). However, owing to the increased complexity of the necessary adjustments, it is not conducive for practical use. BSRF researchers have successfully simplified DEI with only two crystals, one creating monochromatic synchrotron radiation and the other working as an analytic crystal in the Bragg mode (Li *et al.*, 2004, 2005). In this study the monochromator and analytic crystals used were Si (111) single crystals with an X-ray energy of 9 keV. The sample was placed between these crystals along the X-ray beamline, and the CCD detector, with a 10 μm pixel size, was positioned behind the analytic crystal.

In-line holographic imaging uses X-rays with spatial coherence and records the second derivative related intensity change of phase after the X-rays have crossed the sample and then propagate freely into free space (Xu *et al.*, 2001). It has become one of the more promising methods as it is based on a simple principle with an easy feasibility and is technically less demanding. However, the basic requirement is that the incident X-rays must have a good spatial coherence and the distance from the detector to the sample needs to meet a certain requirement. In this experiment the X-ray energy used was 9 keV, the horizontal and vertical spatial coherence length was approximately 7 μm and 21 μm, respectively, the distance from the detector to the sample was 50 cm, and the CCD imaging detector had a spatial resolution of 10 μm.

3. Results

3.1. Imaging of mucosa surface

On in-line holography images performed by synchrotron-radiation broadband monochromatic light, all of the specimens displayed a diffuse spot-like bright area on the normal mucosa surface *in vitro* [Fig. 1(*a*), white arrow]. The spot-like area was uniform with a diameter of 50–70 μm, which was concordant with the shape of the gastric pit under a light microscope (Fig. 1*d*). The line-like bright structure [Fig. 1(*a*),

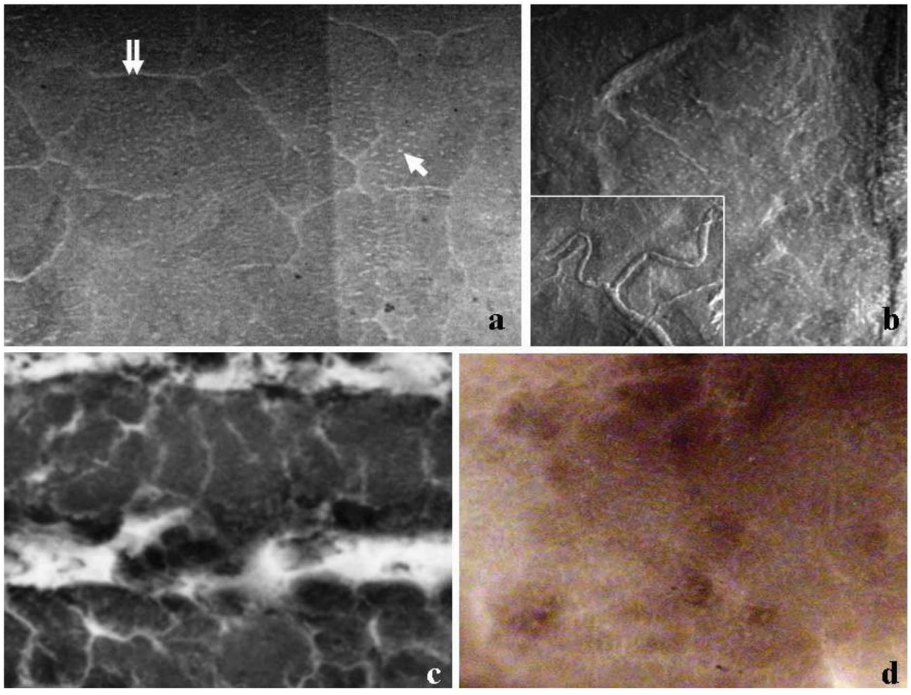

Figure 1
SR-PCI of the gastric mucosa layer. (*a*) In-line holography displaying the gastric pit (white arrow), gastric groove (double arrow) and gastric area enclosed by gastric grooves. (*b*) DEI demonstrating the gastric pit and blood vessels in the submucosa layer (low left). (*c*) Conventional X-ray absorption imaging of the gastric mucosa coated by barium sulfate, which could only demonstrate the gastric grooves. (*d*) Light-microscope images displaying the shape of the gastric pit, as for SR-PCI but more vague than the latter.

double arrow] of the gastric groove split the mucosa into several parts, namely the gastric area. On DEI, the stereoscopic impression of the gastric pit and groove was enhanced, and small vessels under the mucosa were shown (Fig. 1*b*). The same specimen was investigated by conventional absorption X-ray imaging after coating with barium sulfate, but only the shape of the gastric grooves was displayed and no gastric pit was visible (Fig. 1*c*).

On the mucosa surface of the cancerous part (Fig. 2), a fibrous scar at the bottom of a malignant ulcer was shown as a transverse ribbon-like protrusion on DEI (black arrow). The annular dike was displayed clearly as a circular protrusion, and a regional irregular border was displayed as a cause of cancer penetration (white arrow), proposing a Borrmann type-3 gastric cancer.

3.2. Imaging of a cross-sectional specimen

Cross-sectional images of the normal gastric wall demonstrated a three-layer structure on DEI (Fig. 3), which were the mucosa layer (inner dark layer), submucosa layer (middle bright layer) and muscular layer (outer dark layer). The cancer tissue infiltrating the submucosa layer was clearly depicted as an area of opacity (five pointed star).

4. Discussion

Our SR-PCI experiment on gastric *in vitro* specimens at beamline 4W1A of BSRF demonstrates that SR-PCI can depict the gastric pit, which measured only 50–70 µm and appeared as a diffuse spot-like bright area on the normal mucosa surface with a clear border. The gastric pits clustered together and were divided by crossing bright lines (gastric grooves) into several regions measuring 1–3 mm, whose counterpart was the smallest structure that can be displayed by conventional X-ray double-contrast imaging (gastric area). The gastric pit cannot

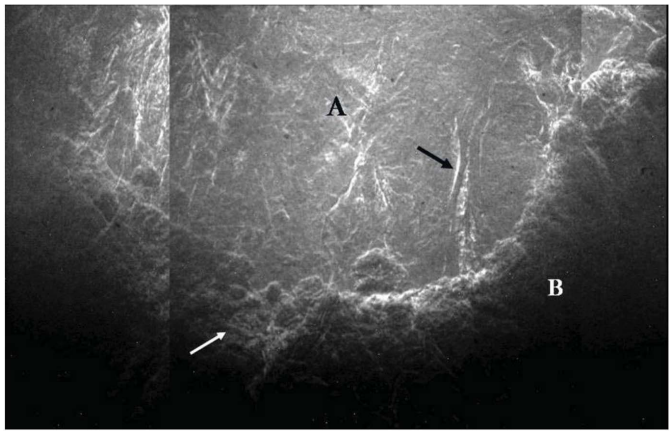

Figure 2
SR-PCI (DEI) of the mucosa surface of gastric cancer. *A*: bottom of a malignant ulcer. *B*: annular dike. White arrow: the penetrating area of the annular dike, proposing a Borrmann type-3 gastric cancer; black arrow: a transverse fibrous scar at the bottom of an ulcer.

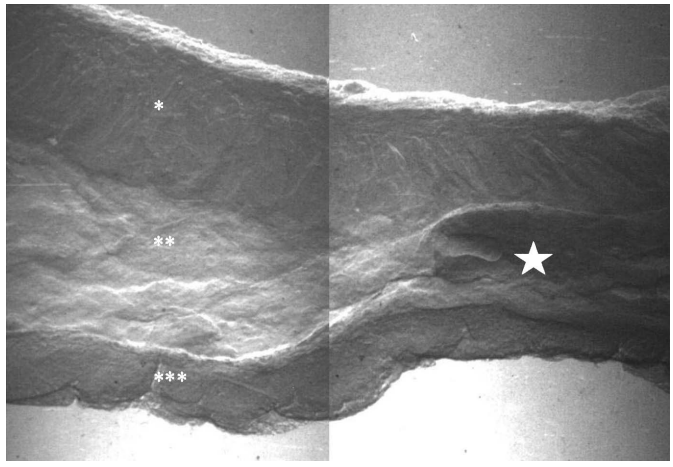

Figure 3
SR-PCI (DEI) of the border between the normal gastric wall and gastric cancer. *: Mucosa layer; **: submucosa layer; ***: muscularis propria; large white star: gastric cancer infiltrating the submucosa layer.

be displayed by conventional X-ray double-contrast imaging. Although a light microscope can display the shape of the gastric pit *in vitro*, owing to imaging by visible light, its penetrating ability is limited and it is far less clear than SR-PCI in demonstrating gastric pits and grooves.

Amplifying electronic gastroscopy is the only modality that can be used to observe gastric pits *in vivo* at present. It is generally considered that gastric pits appear in several different forms such as spots, lines, patches and feathers, depending on their position or the pathologic status of the gastric mucosa (Bruno, 2003). The spot-like type is the most prevalent, which coincides with our study using SR-PCI. The downside of amplifying electronic gastroscopy is the invasive and uncomfortable experiences of the patients during examination. Limited by the orientation of stomach distension, the display of some parts of the stomach, such as the cardiac and posterior wall of the fundus, is usually unsatisfactory, and demonstration of IIb early gastric cancer also has limitations (Han *et al.*, 2003). Owing to the improvement of imaging resolution with SR-PCI, the possibility of using X-rays to analyze tiny structures of the gastric mucosa has become a reality. Computed tomography imaging using the SR-PCI technique has also shown developments recently (Sun *et al.*, 2007), and the combination of these two modalities will provide useful information for the imaging of gastric cancers and precancerous lesions.

In our studies, tiny blood vessels under the gastric mucosa could be clearly displayed by DEI, which were difficult to display using other modalities. The demonstration of feeding blood vessels of cancer is important in the evaluation of gastric cancer. Angiogenesis plays an important role in the course of generation, development, infiltration and metastasis, and influences the biological behaviour and prognosis of gastric cancer (Yao *et al.*, 2010). Owing to low resolution, conventional X-ray computed tomography cannot be used to observe the inner blood vessel structures directly. Contrast agents need to be injected through vessels to improve the contrast and to reflect the blood supply of cancer indirectly (Yao *et al.*, 2010). In this study we used SR-PCI to display the tiny blood vessels that measured only several tens of micrometres without the assistance of a contrast agent, which may provide further information for gastric cancer imaging.

The SR-PCI imaging of gastric cancer in the mucosa plane clearly displayed a fibrous scar at the bottom of an ulcer, the shape and boundary of the annular dike, and a penetrating area, measuring only 2 mm, of the annular dike. All of the above signs could provide useful information for the classification of gastric cancer. The imaging of a cross-sectional specimen demonstrated the three-layer structure of the gastric wall and depicted the infiltration of cancerous tissue in the gastric wall, which may be helpful in the T-staging of gastric cancer.

Our study has several potential limitations. First, we performed a comparison between phase-contrast imaging and conventional hospital imaging apparatus in order to provide direct information about their performances; however, variations in the detectors may contribute to the differences. Second, this imaging technique still cannot be used *in vivo*; we designed this *in vitro* study in order to show the possibility for future use. Also, high-resolution detail may be lost because of the overlap of organs *in vivo*, so further studies are needed to address the clinical value of this method.

In conclusion, SR-PCI can clearly depict gastric pits and grooves without the help of barium sulfate, and can display tiny blood vessels in the submucosa layer without the help of a contrast agent. Demonstrations of the fine structure of a cancerous ulcer and the gastric wall layer, plus the cancer infiltration, all provide useful information for the diagnosis of gastric cancer. Although this technique is presently not applicable in clinical practices, the potential application displayed by this research may propose a new direction for the future imaging of gastric cancer.

This work was supported by the National Basic Research Program of China (973 Program) (grant No. 2011CB707705), the National Natural Science Foundation of China (grant No. 30970825) and the Natural Science Foundation of Beijing, China (grant No. 7092020).

References

Bruno, M. J. (2003). *Gut*, **52**, 7–11.
Dilmanian, F. A., Zhong, Z., Ren, B., Wu, X. Y., Chapman, L. D., Oriont, I. & Thomlinson, W. C. (2000). *Phys. Med. Biol.* **45**, 933–946.
Han, J. Y., Son, H., Lee, W. C. & Choi, B. G. (2003). *Med. Oncol.* **20**, 265–269.
Keyriläinen, J., Fernández, M., Fiedler, S., Bravin, A., Karjalainen-Lindsberg, M. L., Virkkunen, P., Elo, E. M., Tenhunen, M., Suortti, P. & Thomlinson, W. (2005). *Eur. J. Radiol.* **53**, 226–237.
Kitchen, M. J., Paganin, D., Lewis, R. A., Yagi, N., Uesugi, K. & Mudie, S. T. (2005). *Nucl. Instrum. Methods Phys. Res. A*, **548**, 240–246.
Li, G., Chen, Z. H., Wu, Z. Y., Ando, M., Pan, L., Wang, J. & Jiang, X. (2005). *Nucl. Instrum. Methods Phys. Res. A*, **548**, 200–206.
Li, G., Wang, N. & Wu, Z. Y. (2004). *Chin. Sci. Bull.* **49**, 2120–2125.
Liu, P., Sun, J., Guan, Y., Yue, W., Xu, L. X., Li, Y., Zhang, G., Hwu, Y., Je, J. H. & Margaritondo, G. (2008). *J. Synchrotron Rad.* **15**, 36–42.
Muto, H., Matsuura, K. & Hayakawa, H. (2001). *Nippon Igaku Hoshasen Gakkai Zasshi*, **61**, 721–729.
Oltulu, O., Zhong, Z., Hasnah, M., Wernick, M. N. & Chapman, D. (2003). *J. Phys. D*, **36**, 2152–2156.
Parkin, D. M., Bray, F., Ferlay, J. & Pisani, P. (2005). *CA Cancer J. Clin.* **55**, 74–108.
Reto, M., Yeukuang, H., Jung, H. J. & Margaritondo, G. (2004). *Eur Radiol.* **14**, 1550–1560.
Sun, Y., Zhu, P., Yu, J. & Chen, X. (2007). *Comput. Med. Imaging Graph.* **31**, 383–389.
Takeda, T., Momose, A., Hirano, K., Haraoka, S., Watanabe, T. & Itai, Y. (2000). *Radiology*, **214**, 298–301.
Takeda, T., Momose, A., Ueno, E. & Itai, Y. (1998). *J. Synchrotron Rad.* **5**, 1133–1135.
Virkkunen, P. & Retulainen, M. (1980). *Gastrointest. Radiol.* **5**, 325–329.
Xu, W., Jericho, M. H., Meinertzhagen, I. A. & Kreuzer, H. J. (2001). *Proc. Natl Acad. Sci. USA*, **98**, 11301–11305.
Yagi, N., Suzuki, Y., Umetani, K., Kohmura, Y. & Yamasaki, K. (1999). *Med. Phys.* **26**, 2190–2193.
Yao, J., Yang, Z. G., Chen, T. W., Li, Y. & Yang, L. (2010). *Abdom Imaging.* 35, 195–202.